View metadata, citation and similar papers at core.ac.uk

brought to you by CORE

provided by Elsevier - Publisher Connector

Chemistry & Biology, Vol. 9, 79–92, January, 2002, ©2002 Elsevier Science Ltd. All rights reserved. PII S1074-5521(01)00096-5

Hepatitis C Virus NS3 Protease Requires Its NS4A Cofactor Peptide for Optimal Binding of a Boronic Acid Inhibitor as Shown by NMR

Sharon J. Archer, Daniel M. Camac, Zhongren J. Wu, Neil A. Farrow, Peter J. Domaille, Zelda R. Wasserman, Marina Bukhtiyarova, Christopher Rizzo, Sharada Jagannathan, Lawrence J. Mersinger and Charles A. Kettner[1,2]
DuPont Pharmaceuticals Company
Wilmington, DE 19880

Summary

NMR spectroscopy was used to characterize the hepatitis C virus (HCV) NS3 protease in a complex with the 24 residue peptide cofactor from NS4A and a boronic acid inhibitor, Ac-Asp-Glu-Val-Val-Pro-boroAlg-OH. Secondary-structure information, NOE constraints between protease and cofactor, and hydrogen-deuterium exchange rates revealed that the cofactor was an integral strand in the N-terminal β-sheet of the complex as observed in X-ray crystal structures. Based upon chemical-shift perturbations, inhibitor-protein NOEs, and the protonation state of the catalytic histidine, the boronic acid inhibitor was bound in the substrate binding site as a transition state mimic. In the absence of cofactor, the inhibitor had a lower affinity for the protease. Although the inhibitor binds in the same location, differences were observed at the catalytic site of the protease.

Introduction

Hepatitis C virus (HCV) currently infects approximately 3% of the world population and can lead to liver cirrhosis and hepatocellular carcinoma. As with other members of the Flaviviridae family, HCV is a single-stranded positive RNA virus that encodes a large (approximately 3000 amino acid) polypeptide. Maturation of this HCV polypeptide into functional proteins requires cleavage at distinct sites. One of its own protein products, NS3 serine protease (the first 180 residues of NS3), cleaves the HCV polypeptide in the NonStructural region at four junction sites: NS3-NS4A, NS4A-NS4B, NS4B-NS5A, and NS5A-NS5B [1–3]. The nonstructural protein NS4A is required for in vivo cleavage at the NS4B-NS5A site and enhances the cleavage rate at the other sites [4]. Only a portion of NS4A (residues 22′–33′) is necessary for its NS3 cofactor activity, and replacement of the full-length protein by an NS4A peptide is sufficient for enhanced cleavage at junction sites NS4A-NS4B, NS4B-NS5A, and NS5A-NS5B in vitro [5]. Because of the importance of NS3 in the lifecycle of HCV, there has been keen interest in understanding its activation by NS4A.

X-ray crystal structures of NS3 protease in complex with NS4A peptide [6–8] show that the protein adopts a chymotrypsin-like fold with the catalytic triad formed by residues His57, Asp81, and Ser139. In this complex, the protease domain has the same conformation as in a complex of full-length NS3 (protease and helicase domains) with NS4A peptide [9]. The peptide intercalates into the N-terminal domain and forms one strand of the N-terminal β-barrel with the NS3 N-terminal β strand A0 and helix α0 packed against it, whereas in a crystal structure of protease alone, the N-terminal residues (1–30) are extended away from the protein [10]. Thus, the N-terminal domain must undergo substantial rearrangement, as well as additional changes at the active site that optimize the location of residues His57 and Asp81 relative to Ser139 [8]. In the NMR solution structure of NS3 protease alone, the C-terminal domain and hydrophobic core resemble the conformation in the binary complex, while the N-terminal β strand A0 and helix α0, which fold along the peptide in the X-ray structure of the complex, are unstructured [11]. Likewise, an engineered single-chain NS4A-NS3 protein in which the NS4A peptide was tethered to the N terminus of NS3 protease via a four-residue linker lacked well-defined structure for the NS4A residues and the first 30 NS3 residues [12]. In this single-chain protein, however, an NOE was identified between NS4A and NS3 (HN-Gly27′ to HN-Ile135), suggesting that NS4A might adopt the conformation seen in the crystal structure of NS3/NS4A. Despite disorder in the N terminus, the presence of NS4A induced proper alignment of the catalytic triad as evidenced by key NOEs and the downfield chemical shift of His57 backbone amide proton [12].

Structural information on the interaction of NS3 and NS3/NS4A with active site inhibitors has provided conformational details of protein/inhibitor interactions. X-ray crystal structures of NS3/NS4A complexed with two α-ketoacid inhibitors (Boc-Glu-Leu-NH-CH(CH_2CHF_2)CO-COOH and Z-Ile-Leu-NH-CH(CH_2CHF_2)CO-COOH) [13] and an NMR solution structure of NS3 with an α-ketoacid inhibitor (Boc-Glu-Leu-NH-CH(CH_2CHF_2)CO-COOH) [14] have been reported. In this series of inhibitors, -CHF_2 acts as a surrogate for -SH of the P_1 Cys of the substrate (per the nomenclature of Schecter and Berger [15], substrate and inhibitor positions are designated as …P_3-P_2-P_1—P_1'-P_2'-P_3'…, with the scissile bond between P_1 and P_1'). The inhibitors are in extended conformations, with Leu and Glu or Ile occupying the P_2 and P_3 binding sites, respectively. The inhibitor carbonyl bonds with the active site serine, Ser139, to form a hemiketal (Figure 1A); the oxyanion is hydrogen bonded to the active site histidine, His57; and the carboxylate occupies the oxyanion hole. This type of interaction has also been observed for ketoacid analogs in complex with thrombin [16]. In contrast, ketoacid inhibitors in complexes with trypsin and thrombin have also been characterized as "reaction intermediate analogs" [17], where R in Figure 1B is a *p*-amidinophenyl group [18]. In these analogs, the carbonyl is likewise bonded to the active site serine, Ser195 (Ser139 in NS3), but the carboxylate and oxyanion are reversed, the former hydrogen bonded to the histidine and the latter in the

[1] Correspondence: charles.kettner@bms.com
[2] Present address: Bristol-Myers Squibb Company, Experimental Station, Wilmington, DE 19880.

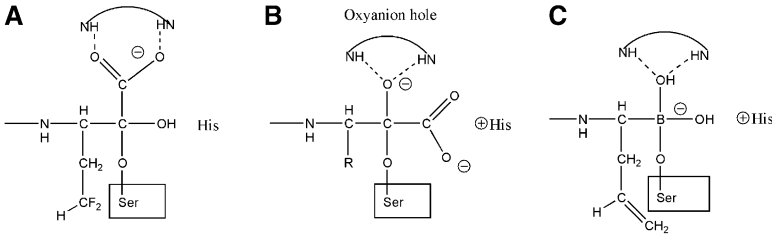

Figure 1. Models of Active Site Inhibitors of Serine Proteases

Schematic representations were based on (A) ketoacid binding as a hemiketal as in the crystal structure of NS3/NS4A/ketoacid inhibitor [13] and the NMR structure of NS3/ketoacid [14], (B) ketoacid binding as a reaction intermediate analog [18], and (C) boronic acid binding as a reaction intermediate analog [19].

oxyanion hole. This configuration mimics the tetrahedral intermediate expected for substrate hydrolysis, in which addition of the active site serine to the carbonyl of the scissile bond results in formation of an acyl enzyme. Structures of α-ketoacid inhibitors in complex with NS3 [14] and with NS3/NS4A [13] showed that this type of transition state analog was not present for these inhibitors. The pKa of the His57 imidazole is less than 5.7 [14] and thus further distinguishes it from a reaction intermediate analog where the histidine would be protonated (Figures 1B and 1C).

Although the high-resolution structures of inhibited protease provide key insights into the binding of ketoacid inhibitors, a good transition state analog would yield additional information relevant to substrate hydrolysis. In crystallographic and NMR studies of boronic acid inhibitors complexed with other serine proteases, the boronic acids can act as "reaction intermediate analogs" [19–22]. The active site serine makes a near tetrahedral adduct with the boronic acid, one borate -OH occupies the oxyanion hole, and the other hydrogen bonds with the histidine (Figure 1C). The active site imidazole ring NH groups are involved in strong hydrogen bonds, and the imidazole has a pKa $>$ 9 [20, 23].

Herein we describe NMR studies of NS3/NS4A in complex with the peptide boronic acid inhibitor, Ac-Asp-Glu-Val-Val-Pro-boroAlg-OH (InhI; boronic acid analog of allylglycine). This inhibitor mimics the sequence of a good substrate for NS3 protease [24] and is expected to bind in the substrate P_6-P_1 binding sites. The allylic side chain is predicted to bind in a manner similar to the -CH_2SH of Cys and the -CH_2CHF_2 side chain of the ketoacid inhibitors. The allylic proton is polarized and can potentially interact with the aromatic ring of Phe154 in the bottom of the P_1 pocket [24].

To date, NMR studies of NS3 protease inhibitors have examined peptidic inhibitors in solution [25] and when bound to NS3 [26–28]. NMR studies have also elucidated the full three-dimensional structure of NS3 protease alone [11] and in complex with ketoacid inhibitors [14] but not with bound NS4A cofactor. We have found sample conditions that optimize the affinity of cofactor for protease, enabling the inhibitor-protease interactions to be studied in solution with bound cofactor. Both the protease and cofactor were enriched with ^{15}N and ^{13}C isotopes, and backbone resonances were assigned for both NS3 and NS4A in the NS3/NS4A/inhibitor complex. We determined the effect of cofactor on inhibitor binding by comparing spectra of the protease in various states: NS3, NS3/NS4A, NS3/inhibitor, and NS3/NS4A/inhibitor. The interpretation of the NMR data is based on published structures and an NS3/NS4A/inhibitor model presented herein.

Results and Discussion

Complex Formation

Because NS4A is critical for the activity of NS3 protease, we searched for protein and cofactor constructs that allowed NMR study of the high-affinity complex. ^{1}H-^{15}N HSQC (heteronuclear single-quantum correlation) spectra [29] were used to monitor changes in chemical shifts of NS3 that result from interactions with the cofactor peptide. Based on a construct used in crystal complexes [7], spectra of proteases from the 1b genotype showed no changes upon addition of peptide 1b-16mer or the longer 1b-23mer (Table 1). Increasing the glycerol concentration (10% v/v) enhanced peptide affinity, in agreement with previous reports [30, 31], but resulted in poorer quality NMR spectra because of increased viscosity.

For protease from the 2a genotype, the addition of NS4A peptide (1b-16mer or the longer 1b-23mer [Table 1]) resulted in improvements in peak dispersion and substantial chemical-shift changes, consistent with complex formation (Figure 2). On the other hand, the addition of peptides based on the 2a genotype (2a-18mer or 2a-23mer [Table 1]) caused no spectral changes, implying low affinity for the protease. The ability of the 2a protease to bind peptides from other genotypes more tightly than its cognate cofactor is in agreement with a report that NS3 2a protease activity was stimulated more effectively by NS4A from alternate genotypes [32]. In all subsequent experiments, NS3 2a and NS4A 1b-23mer (or 1b-24mer) were used, a combination that provided well-dispersed HSQC spectra in 2% glycerol.

The ^{1}H-^{15}N HSQC spectrum of the ^{15}N-NS3/NS4A complex showed uniform linewidth peaks and good chemical-shift dispersion indicative of a folded protein (Figure 2). However, at the concentrations required for spectral

Table 1. NS4A Cofactor Peptide Sequences

Peptide	Sequence
1b-16mer[a]	KGSVVIVGRIILSGRK
1b-23mer[b]	KKGSVVIVGRIVLSGKPAIIPKK
1b-24mer[c]	KKGSVVIVGRIVLSGKPAIIPKKhS
2a-18mer[d]	KKGSVSIIGRLHVNQRKK
2a-23mer[d]	KKGCVCIIGRLHVNQRAVVAPKK

[a] The peptide sequence from the 1b genotype which was used in the crystallographic studies described in reference [7].
[b] The peptide sequence from the 1a/1b genotype that was used in the crystallographic studies described in reference [6].
[c] This peptide was prepared isotopically enriched.
[d] These peptides correspond to the sequence of NS4A from the 2a genotype.

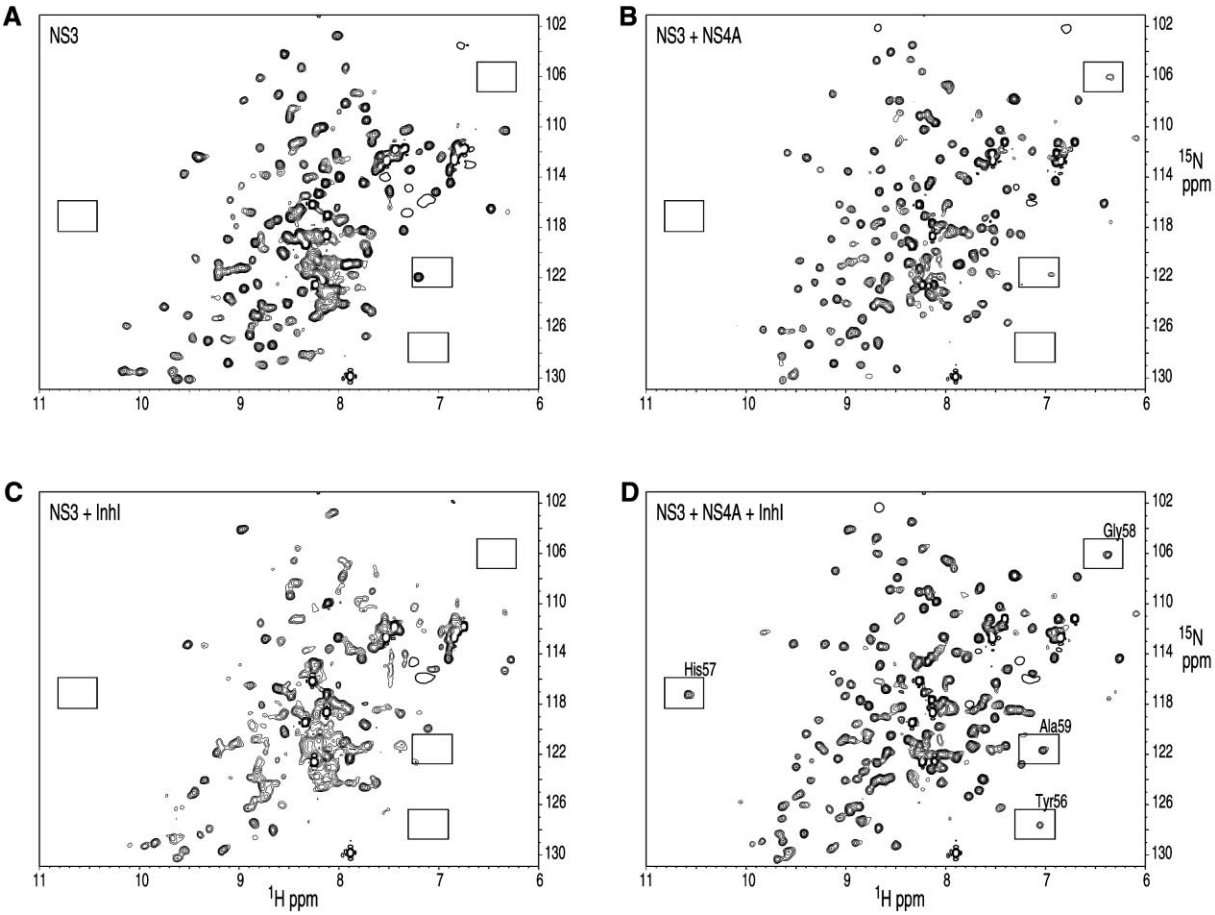

Figure 2. ^{1}H-^{15}N HSQC Spectra NS3 Protease Complexes

(A) ^{15}N-NS3.

(B) ^{15}N-NS3/NS4A.

(C) ^{15}N-NS3/InhI.

(D) ^{15}N-NS3/NS4A/InhI.

Positive and negative peaks are depicted by eight and one contours, respectively. Samples for spectra (A), (C), and (D) were prepared sequentially by starting with (A) 150 μM ^{15}N-NS3 2a (1–192) in 25 mM MES (pH 6.5), 100 mM NaCl, 5 mM DTT, 2% glycerol, 6% D_2O, adding (C) 250 μM InhI, and subsequently adding (D) 160 μM NS4A. Alternating the order of addition (first adding NS4A then InhI) resulted in a spectrum identical to (D). The sample for (B) contained 110 μM ^{15}N-NS3 and 135 μM NS4A in the above buffer. All spectra were acquired with 64 transients, 64 complex increments in t_1 (^{15}N), 256 complex points in t_2 (^{1}H), and spectral widths of 1886.79 Hz in t_1 and 9259.26 Hz in t_2, with the ^{1}H carrier set on the water resonance and the ^{15}N carrier set at 116 ppm. Spectral regions surrounding labeled peaks are boxed to aid visual comparison between spectra.

assignments, significant line broadening was observed, and autoproteolysis (detected via SDS-Page gels and mass spectrometry) occurred at unacceptable rates.

Addition of the peptidic boronic acid inhibitor, Ac-Asp-Glu-Val-Val-Pro-boroAlg-OH, stabilized the complex against autoproteolysis so that the protein concentration could be increased to 1 mM, suitable for NMR resonance assignments. The quality of the ^{1}H-^{15}N HSQC spectrum reflects a well-folded protein complex (Figure 2). At less than one equivalent inhibitor, separate peaks were seen for bound and free protein, indicating that the inhibitor did not dissociate from the complex on the NMR time scale. At approximately one equivalent of inhibitor, the number and linewidth of the peaks imply a firm inhibitor bound complex. Even under the optimized sample conditions, there was some degradation in spectral quality upon concentration of the sample from 180 to 800 μM. The ^{15}N spin-spin relaxation time (T_2) decreased from 52 to 44 ms, likely reflecting partial sample aggregation.

Protein constructs used in the NS3 solution structures [11, 14] have a C-terminal poly-lysine tag, whereas the single-chain NS4A-NS3 construct does not [12]. We have used an NS3 2a (1-181)Lys_6 construct to acquire a duplicate set of spectra in addition to those described above. Similar spectral changes were observed, suggesting that the C-terminal tag does not affect cofactor or inhibitor binding.

The NS4A cofactor peptide was examined with and without protease to detect conformational changes in the peptide upon binding. The ^{1}H-^{15}N HSQC spectrum of ^{15}N-enriched NS4A in solution displayed little chemical-shift dispersion, characteristic of an unstructured peptide (Figure 3A), whereas binding to NS3 and inhibitor

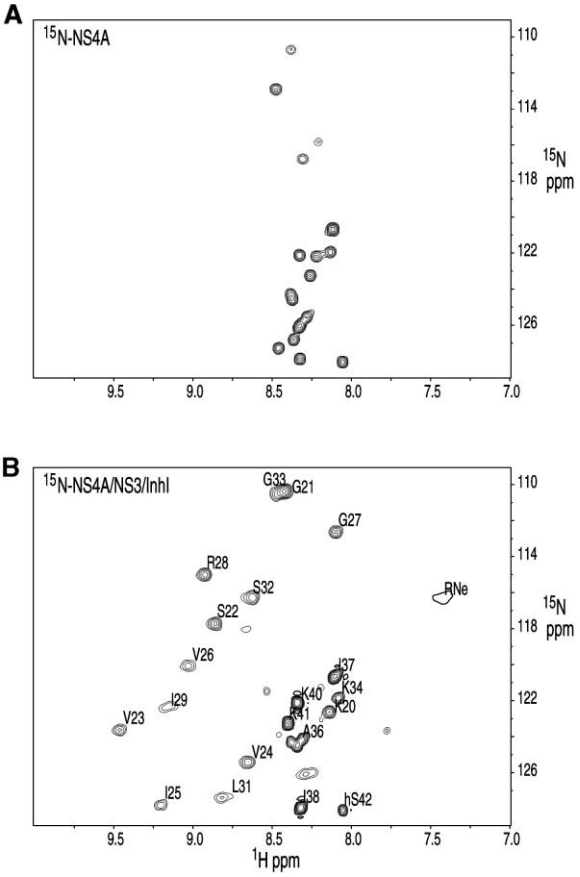

Figure 3. NMR Spectra of NS4A Cofactor Peptide

^{1}H-^{15}N HSQC spectra of (A) 900 μM ^{15}N-NS4A and (B) 115 μM ^{15}N-NS4A/NS3/InhI acquired with the parameters listed in Figure 2. Amide assignments are shown for NS4A in the NS3/NS4A/InhI complex. Note that amide peaks for C-terminal residues I237–hS242 overlap with peaks from unbound NS4A.

resulted in increased chemical-shift dispersion (Figure 3B). This is consistent with the peptide adopting a well-defined conformation within the complex.

Enzymatic Characterization of NS3/NS4A Complex

The protease complex was characterized by measuring the cleavage of a peptide substrate, Ac-Asp-Glu-Asp(Edans)-Glu-Glu-AbuΨ[COO]Ala-Ser-Lys(Dabcy)-NH_2 [33]. Figure 4A shows the catalytic activity of the NS3/NS4A complex as a function of substrate concentration (2.5–200 μM). A linear dependence of velocity versus substrate concentration was obtained and indicated that the K_m was greater than 50 μM. From the slope of this plot, k_{cat}/K_m was found to be $5.4 \times 10^5 \pm 1.3 \times 10^4$ $M^{-1}s^{-1}$.

Catalytic activity was highly dependent on the presence of the NS4A cofactor. As shown in Figure 4B, NS3 was approximately 50-fold less active in the absence of NS4A. We determined the dissociation constant for the NS3/NS4A complex by measuring enzymatic activity as a function of NS4A concentration (Figure 4C). The equation describing the reaction velocity, $v = V_{max}[NS4A]/K_d + [NS4A]$, fit the data with a maximum velocity, V_{max}, of 0.075 ± 0.007 μmol/l/min and a dissociation constant, K_d, of 2.4 ± 0.8 μM. Finally, the affinity of NS3/NS4A for InhI was determined (Figure 4D). The equation $vi/vo = 1/(1 + [Inh]/K_iapp)$, where vi and vo are the velocities in the presence and absence of inhibitor and $K_i$app (K_i apparent) is $K_i(1 + [S]/K_m)$, gave a good fit to the data. Since the concentration of substrate, S, is 5.0 μM and K_m is greater than 50 μM (Figure 4A), $K_i$app is equivalent to K_i(13 ± 2 nM) for competitive inhibition.

The binding of InhI to NS3 in the absence of NS4A was also studied. Under conditions similar to those described in Figure 4D, we determined the inhibition of NS3 (100 nM) by using 500–1000 nM InhI levels. Between 6% and 26% inhibition was observed. This range of inhibition was limited in order to maintain pseudo-first-order reaction conditions. Handling the data in the same manner as described in Figure 4D gave a $K_i$app = 160 ± 35 nM (n = 5).

Resonance Assignments and Secondary Structure

NMR resonance assignments of the protease and peptide are necessary in order to map observed NMR spectral changes to specific residues in the protein. Because the NS3/NS4A binary complex was susceptible to autoproteolysis, the resonance assignments were determined with the inhibitor bound. Backbone resonance assignments were determined for ^{15}N,^{13}C-NS3 and for ^{15}N,^{13}C-NS4A in an NS3/NS4A/InhI complex with CBCACONH, HNCACB, and HNCA triple resonance experiments (Table 2) following well-established strategies [34, 35]. Resonances were assigned for 95% of the backbone H_N, N, Cα, and Cβ atoms for residues Thr4 to Ser181 of NS3 and for all residues of NS4A, with the exception of the N-terminal Lys19′ and the amides of Lys20′ and Val30′.

Secondary-structural elements were identified with the chemical shift index (CSI) [36], where contiguous stretches of large positive deviations Δδ(Cα) are indicative of α helices and large negative Δδ(Cα) and positive Δδ(Cβ) are representative of β strands (Figures 5A and 5C). Of particular note were the CSIs that clearly delineate the N-terminal β strand A0 and helix α0 (Figure 5A). This strand and helix are present in X-ray crystal structures of NS3/NS4A binary complexes [6–8], but in NMR studies of the single-chain complex in solution, there is no evidence of helix α0 [12]. Neither A0 nor α0 is observed in NMR [11] and crystallographic [10] structures of NS3 alone. In our complex, strong sequential amide-amide NOEs for residues Leu14–Arg24 provide additional evidence for the existence of a helical structure, α0 (data not shown).

Most β strands were identified by both Δδ(Cα) and Δδ(Cβ) (Figure 5A). The CSI analysis also suggested the existence of an additional strand for residues 91–95; although this region is not a β strand in the crystal structure, it is relatively extended. The only NS3 secondary-structural element observed in the crystal structures that was not identified by the CSI methodology was the α1 helical turn. However, Tyr56, His57, and Ala59 had Cα shifts consistent with a helix (although Gly58 did

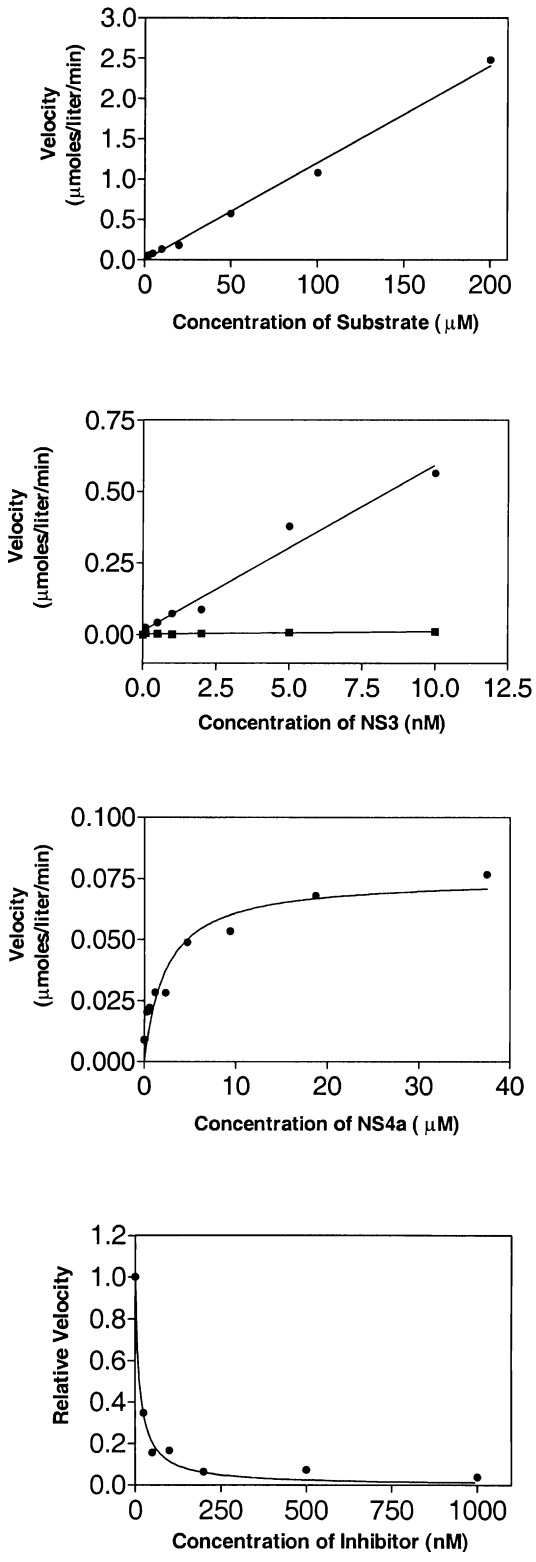

Figure 4. Enzymatic Characterization of the Protease

(A) Substrate hydrolysis rates as a function of substrate concentration. NS3 (0.38 nM) was incubated with 10 μM NS4A for 5 min at pH 7.0 and 25°C. Substrate, Ac-Asp-Glu-Asp(Edans)-Glu-Glu-AbuΨ[COO]Ala-Ser-Lys(Dabcy)-NH_2, was added to the final concentration indicated on the *x* axis. Hydrolysis rates were determined via HPLC (see Experimental Procedures).

not), and residues His57–Ala59 had amide-amide NOEs consistent with the helical turn.

For NS4A, the $\Delta\delta(C\alpha)$ and $\Delta\delta(C\beta)$ values were predominantly negative and positive, respectively, indicating that the peptide adopts a β strand conformation when it is bound to protease (Figure 5C). Strict adherence to the CSI approach for both Cα and Cβ shifts delineates a β strand only from residue Arg28′–Ser32′, although several other residues had shifts that were strongly suggestive of a longer β strand. Overall, the secondary-structural elements identified in this study are in agreement with those reported in the NS3/NS4A crystal structure, and the minor discrepancies reflect a limitation of this statistical method rather than significant conformational differences [36].

H_N-H_N crosspeaks between the peptide and protease were measured in a ^{13}C-filtered, ^{15}N-selected NOE spectroscopy (NOESY) experiment on $^{15}N,^{13}C$-NS3/$^{15}N,^{13}C$-NS4A/InhI. NOE crosspeaks were observed between NS3 and NS4A amide protons for Gln8–Arg28′, Gln32–Ile29′, Val33–Ile29′, Val35–Gly27′, Ser37–Val24′, and Ala65–Val23′. These six intermolecular NOEs were consistent with short (< 4 Å) interproton distances predicted by the crystal structure (PDB code 1jxp) [7] (modeled with hydrogens added) and are sufficient to orient NS4A relative to NS3. In addition, a strong intramolecular NOE between the amides of Val26′ and Gly27′ in NS4A suggests a short interproton distance; in the crystal structure, a small kink in the middle of the strand brings the amide protons of Val26′ and Gly27′ into close proximity. From the crystal structure, NOEs would also be expected between Tyr6 and Val30′ and between Thr4 and Ser32′; these could not be identified because the amide of Val30′ is unassigned and the amide protons of Thr4 and Ser32 are degenerate. The good correlation between NOEs from NMR data and short distances in the crystal structure implies that the bound peptide adopts a similar conformation in solution as in the X-ray crystal structures of NS3/NS4A [6–8].

Our complex appears to maintain more structure in the N terminus than the single-chain NS4A-NS3 1a. Virtually complete resonance assignments were determined for the protease and the peptide, whereas assignments were missing for almost all residues between Ile3 and Val33 of the single-chain construct and only 3 of the 12 residues in the NS4A segment could be assigned [12].

(B) Comparison of catalytic activities of NS3 in the presence and absence of NS4A. NS3 (0.38 nM) was incubated for 10 min in the presence (squares) and absence (circles) of 10 μM NS4A at pH 7.0 and 25°C. Substrate was added to give a final concentration of 5.0 μM, and enzymatic activity was monitored by measuring the increase in fluorescence with time.

(C) Hydrolysis rates as a function of NS4A concentration. The activity of NS3 (1.0 nM) was measured in the presence of varying amounts of NS4A as described in (B). The equation, velocity = V_{max}[NS4A]/K_d + [NS4A], where V_{max} is the maximum velocity and K_d is the dissociation constant, was fit to the data. The following values were obtained: K_d = 2.4 ± 0.8 μM and V_{max} = 0.075 ± 0.007 μmol/l/min.

(D) Effect of InhI on NS3 activity. The activity of NS3 (+NS4A) at varying concentrations of InhI (Ac-Asp-Glu-Val-Val-Pro-boroAlg-OH) was determined as described in (B) except that a NS3 concentration of 5.0 nM was used.

Table 2. NMR Data Acquisition Parameters for All Experiments

Experiment	Dimensions	Spectral Width (Hz)	Carrier (ppm)	Acq. Time (ms)	Complex Points	Transients	Reference
2D ^{1}H-^{15}N HSQC	^{15}N-f1	1,886.79	116.0	33.9	64	64	[29, 61]
	^{1}H-f2	9,259.26	4.773	27.6	256		
2D ^{1}H-^{15}N HSQC	^{15}N-f1	5,000.00	180.0	6.4	32	128	[29, 61]
	^{1}H-f2	19,230.77	4.773	26.6	512		
2D ^{1}H-^{15}N LR-HSQC[a]	^{15}N-f1	1,886.79	180.0	28.2	256	256	[43]
	^{1}H-f2	9,259.26	4.773	27.6	256		
3D CBCA(CO)NH[b,c]	^{13}C-f1	9,615.39	46.0	5.8	56	32	[62, 63]
	^{15}N-f2	1,886.79	116.0	24.4	46		
	^{1}H-f3	9,259.26	4.773	27.6	256		
3D HNCACB[b,c]	^{13}C-f1	9,615.39	46.0	5.0	48	32	[64–66]
	^{15}N-f2	1,886.79	116.0	24.4	46		
	^{1}H-f3	9,259.26	4.773	27.6	256		
3D HNCA[b]	^{13}C-f1	4,000.00	56.0	12.0	48	32	[69, 68]
	^{15}N-f2	1,886.79	116.0	24.4	46		
	^{1}H-f3	9,259.26	4.773	27.6	256		
3D HNCO[b,d]	^{13}C-f1	2,500.00	176.0	16.8	42	32	[67]
	^{15}N-f2	1,886.79	116.0	22.3	42		
	^{1}H-f3	9,259.26	4.773	27.6	256		
3D ^{13}C-filtered, ^{15}N-selected NOESY[c,e]	^{1}H-f1	8,196.72	4.773	15.6	128	16	[69]
	^{15}N-f2	1,886.79	116.0	26.9	32		
	^{1}H-f3	9,259.26	4.773	27.6	256		

[a] Long-range HSQC with 22 ms delay for evolution of $^{1}H_{C}-^{15}N$ couplings.
[b] Acquired on ^{15}N,^{13}C-NS3 2a(1–181)Lys$_6$/NS4A/InhI.
[c] Acquired on ^{15}N,^{13}C-NS3 2a(1–181)Lys$_6$/^{15}N,^{13}C-NS4A/InhI.
[d] Acquired in the presence and absence of inhibitor.
[e] Acquired with a 100 ms mixing time.

The higher degree of structure in our NS3 2a complex relative to the single-chain 1a protein may be due to amino acid differences between constructs or due to the linkage of NS4A to the N terminus of NS3 in the single-chain construct. The latter explanation seems less plausible since single-chain NS4A-NS3 is considerably more active than its binary complex, implying that the linkage is advantageous [37]. Thus, we attribute our more regular secondary structure in the N terminus to differences in primary sequence. This conclusion is supported by our observation that NS3 2a has a higher cofactor affinity than NS3 1b, whose sequence is more similar to that of NS3 1a (see the section titled, "Complex Formation"). This is also consistent with reports on NS3 1b constructs in which the dissociation constants for the protease-peptide complexes are dependent on NS3 sequence [31]. In this same study, the first 21 residues of NS3 1b exhibited high proteolytic susceptibility in the N terminus with and without cofactor, suggesting flexibility in this region even in the presence of cofactor [31]. It has been postulated that the structured N terminus previously observed only in crystal structures may require crystal contacts [31, 12]; our data are consistent with a well-structured NS3 2a N terminus without these stabilizing interactions.

The chemical-shift and NOE data reported here were obtained with bound inhibitor that may contribute to ordering the N terminus of the protein. In the literature, limited proteolysis studies on NS3 1b have shown that the addition of inhibitor increased stability in both the N-terminal and C-terminal domains of the protein [38]. In our studies of NS3 2a, inhibitor was apparently not necessary for a structured N-terminal domain because a protease/peptide complex was achieved without inhibitor (Figure 2B). The amide chemical shifts for residues in β strand A0 and helix α0 were insensitive to inhibitor binding (Figure 5B), demonstrating that the backbone conformations of these N-terminal residues were not perturbed by the inhibitor.

Solvent Accessibility of NS4A Bound to NS3

Hydrogen-deuterium exchange experiments were used to identify protons that were well protected from exchange with water in the NS3/NS4A/InhI complex. In these experiments, a protein sample in H_2O buffer is exchanged into D_2O buffer before acquisition of a ^{1}H-^{15}N HSQC; amide protons protected from solvent are then observable, whereas exchangeable protons are not. A third of the NS3 amide protons were observable after 30 min at 25°C in D_2O, and two-thirds of these were still detectable after an additional 16 hr. This persistence reflects a globular, well-folded protein.

In the N-terminal domain, the amide protons of residues 33–37 (β strand A1) and residues 23′–27′ and 29′ (β strand D1′ of NS4A) were in slow exchange. Based on the published crystal structure (PDB code 1jxp) [7], hydrogen bonds would be expected between the amides of NS3 residues Val33, Val35, and Ser37 and the carbonyls of NS4A, whereas amides of Val24′, Val26′, Gly27′, and Ile29′ would be hydrogen bonded to the carbonyls of β strand A1. The slow exchange rates of the Val23′ and Ile25′ amides are in accord with their buried state predicted by the crystal structure [7]. The amide of Arg28′ in NS4A, hydrogen bonded to the car-

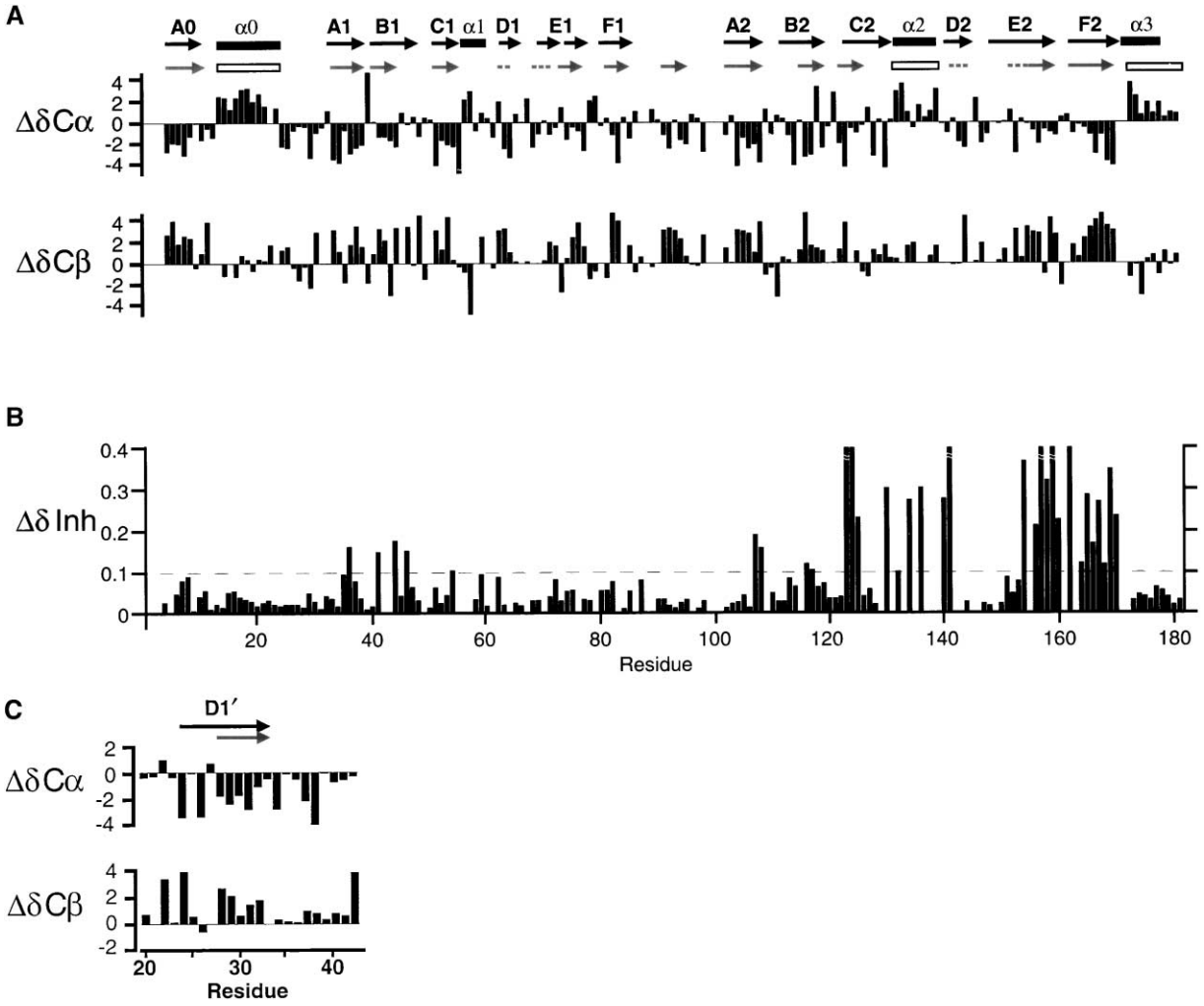

Figure 5. Summary of Secondary Structure and Chemical-Shift Perturbations for NS3/NS4A/InhI

(A) $\Delta\delta$ $^{13}C\alpha$ and $\Delta\delta$ $^{13}C\beta$ were calculated by subtracting the random coil values from the measured $^{13}C\alpha$ and $^{13}C\beta$ chemical shifts for ^{15}N,^{13}C-NS3/NS4A/InhI. Secondary-structure elements as determined from chemical-shift indices according to the method of Wishart and Sykes [36] are depicted as gray arrows for β strands and open rectangles for helices. Secondary-structure features from the NS3/NS4A crystal structure [7] are depicted as black arrows for β strands and solid rectangles for helices.

(B) The weighted chemical-shift perturbations $\Delta\delta Inh = |\Delta\delta^1H| + 0.5*|\Delta\delta^{15}N|$ are calculated for amides of ^{15}N-NS3/NS4A relative to ^{15}N-NS3/NS4A/InhI. Broken bars indicate $\Delta\delta C > 5$ or $\Delta\delta C < -5$ in (A) and $\Delta\delta Inh > 4$ in (B).

(C) $\Delta\delta$ $^{13}C\alpha$ and $\Delta\delta$ $^{13}C\beta$ as described in (A) but for the NS4A peptide in NS3/^{15}N,^{13}C-NS4A/InhI .

bonyl of Gln9 of NS3 in the crystal structure, has a moderate exchange rate and is the only amide facing β strand A0 that is not in rapid exchange. The slow hydrogen-deuterium exchange rates for many amide protons of peptide β strand D1′ and protease β strand A1, along with NOE and chemical-shift data, indicate a strong association between NS4A and NS3.

Although the amide protons in NS4A were in slow exchange, β strand A0 and helix α0 protons that lie alongside the cofactor in the crystal structure were in rapid exchange. These regions adopted regular secondary structure on the NOE time scale (100 ms), whereas on the longer time scale of the hydrogen-deuterium exchange experiment (1000 s), protons in this region were labile. Thus, the N terminus of NS3 2a may not be completely rigid in the presence of cofactor.

Inhibitor Binding Model

We used high-resolution structures of NS3 in solution [11] and NS3/NS4A in crystals [6–8] to interpret our NMR chemical-shift and limited NOE data and to then construct a model of inhibitor binding. The locations of secondary-structural elements and NS4A binding in the ternary complex were in agreement with the published crystal structures, thus justifying the use of these structures in interpreting our NMR data.

Amide chemical-shift perturbations were used to identify the inhibitor binding site. Sample degradation prevented making full assignments on uninhibited protein. As an alternative, the amide assignments for NS3/NS4A utilized 3D HNCO data that were acquired on 0.3 mM protein samples in less than two days. 3D HNCO experiments provide three chemical shifts (H_N, N, and

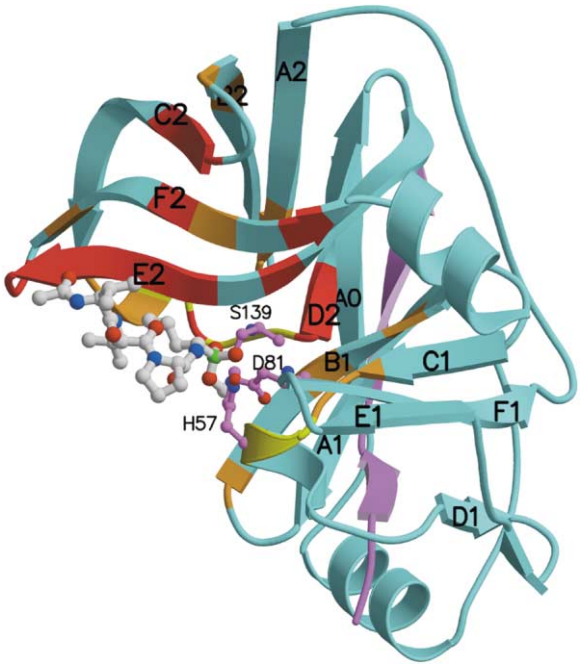

Figure 6. Chemical-Shift Perturbations Mapped onto a Model Structure of NS3/NS4A/InhI

The model was calculated from the crystal structure of NS3/NS4A [7] as described in the text. The inhibitor is depicted in stick representation (white C, blue N, red O, and green B), NS4A (violet) and NS3 are shown as ribbons. The catalytic triad (His57, Asp81, and Ser139) are in stick representation (magenta C, blue N, and red O). Residues whose backbone amide resonances shift more than 0.2 ppm and 0.1–0.2 ppm ($\Delta\delta$Inh in Figure 3B) upon binding InhI are colored red and orange, respectively. Residues Tyr56, His57, Gly137, Ser138, and Ser139, which could not be identified in the absence of InhI, are colored yellow. This figure was generated with Molscript [58] and Raster3D [59].

C′) and allow the correlation of assignments for NS3/NS4A and NS3/NS4A/InhI. Many of the amide assignments could be transferred to the binary complex, enabling measurement of chemical-shift perturbations for a majority of the protease residues (Figure 5B).

Most of the chemical-shift changes occurred in the C-terminal domain, whereas signals from residues of the N-terminal domain that were not directly adjacent to the active site showed little or no perturbation upon inhibitor binding. All of the residues exhibiting large perturbations were located near the loop containing Ser139 and residues 156–159 of β strand E2 (Figure 6), a region that defines the substrate binding site of NS3 protease. The largest changes occurred for residues in the regions 123–125, 136–141, and 154–170 (Figure 5B). The amide resonances for residues of the oxyanion hole (Gly137, Ser138, and Ser139) could not be identified in the absence of inhibitor. This is also the case for α-lytic protease, another serine protease [39], and may be the result of spectral overlap or intermediate chemical exchange in the uninhibited protein. Likewise, the amide peaks for Tyr56 and His57, which are well isolated in the HSQC spectrum of NS3/NS4A/InhI, could not be assigned in the absence of inhibitor (Figure 2). These amide resonances have been assigned for the single-chain NS4A-NS3 1a construct [12] with chemical shifts similar to those of Tyr56 and His57 in our ternary complex. Adjacent residues (for example Gly58 and Ala59, see Figures 2B and 2D) exhibited only moderate chemical-shift changes and were weaker in intensity in the absence of inhibitor. The perturbations were localized near the substrate binding site; the fact that the largest chemical-shift perturbations were on the unprimed side points to that as the location of InhI binding (Figures 5B and 6). This binding site is consistent with published structures of an NS3/ketoacid inhibitor complex in solution [14] and NS3/NS4A/ketoacid inhibitor complexes in crystals [13].

A 3D ^{13}C-filtered, ^{15}N-selected NOE experiment was used to identify NOEs between the inhibitor and the protein backbone. NOE crosspeaks were observed between the inhibitor P_3Val and P_4Val sidechain protons and the amide protons of Ala157 and Cys159, between the inhibitor P_1allyl Hγ and Ala157 amide proton, between the inhibitor P_3Val amide and Ala157 amide protons, and between the P_1allyl Hα and Hβ protons and Gly137 amide proton. These NOEs reflect short distances between the inhibitor and the protein and therefore define the orientation of the bound inhibitor.

To visualize these NOEs, we built a computer model of the inhibitor docked in the unprimed portion of the NS3/NS4A binding site. Coordinates of the protein and its cofactor were based on an energy minimized crystal structure of the 1b construct, PDB code 1jxp [7]. Where necessary, side chains were mutated in accord with the 2a sequence. There are no differences between 1b and 2a protein sequences in the region close to the active site.

The peptide inhibitor used in the model was Ac-Val-Val-Pro-NHCH(CH_2SH)C(OH)-(OCH_3)(γO of Ser139). The two N-terminal acidic residues were not modeled because earlier docking experiments (Z.R.W., unpublished data) indicated that due to numerous positively charged residues abutting the binding site (Arg109, Arg118, Lys119, Arg122, Arg123, Arg130, Lys136, Arg155, Arg161, and Lys165) there were many possible orientations of the N-terminal Asp-Glu, and it was not possible to determine which might be preferred. Previous studies employed cysteine as P_1, and we thought it a suitable substitute for the allyl side chain. In place of boron, we used carbon in a tetrahedral conformation bonded to the γO of Ser139. This necessitated that His57 acquire a proton and be positively charged.

The inhibitor was manually oriented in a position previously determined from computer simulations of related tetrapeptides and peptide mimetics (Z.R.W., unpublished data). The system was then minimized with the program AMBER [40, 41] and further relaxed by 20 ps of molecular dynamics. The simulation made use of AMBER's "belly" option, allowing the inhibitor and most residues within 12 Å of its initial position to move freely except for the protein's main chain atoms, which were constrained with a weak force constant of 1.0 kcal/mol·Å^2. Because of the preponderance and ambiguity of NOE constraints involving the two valine residues of the inhibitor, all three rotamers of each valine were considered as starting conformations, necessitating a total of nine computer runs. The conformations used for analysis were the averages over the last 3 ps of each simulation.

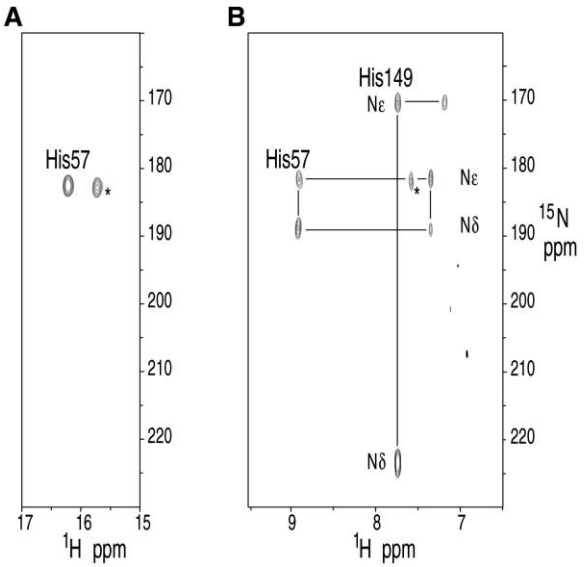

Figure 7. Side Chain HSQC and Long-Range HSQC Spectra of Histidine Imidazole

(A) Imidazole region from ^{1}H-^{15}N HSQC spectrum of 650 μM ^{15}N-NS3/NS4A/InhI in H_2O buffer. The spectrum was acquired with 512 transients, 32 increments in t_1 (^{15}N), 512 complex points in t_2 (^{1}H), and spectral widths of 5000 Hz in t_1 and 19,230.77 Hz in t_2, with the ^{1}H carrier set on the water resonance and the ^{15}N carrier set at 180 ppm.

(B) ^{1}H-^{15}N long-range HSQC spectrum of ^{15}N-NS3/NS4A/InhI in D_2O buffer acquired with the parameters used in (A) except with the ^{15}N carrier centered at 210 ppm, 1024 transients, and a 22 ms delay to allow long-range $^{1}H_C$-^{15}N couplings to evolve. Coupling patterns are depicted for histidine imidazoles.

For comparison with NMR measurements, interactive graphics were used to add hydrogen atoms, and the P_1 cysteine side chain was changed to allyl. In only one of the nine computer models were the inter-atom distances in agreement with the NOE data; that conformation is shown in Figure 6. This model of NS3/NS4A/InhI in conjunction with NMR resonance assignments allows us to interpret our data in the absence of full structure determination.

His57 Imidazole

Chemical shifts of the active site imidazole were used to further characterize the bound state of InhI. In a ^{1}H-^{15}N HSQC spectrum of ^{15}N NS3/NS4A/InhI with the ^{15}N carrier centered at the frequency of the imidazole nitrogens (180 ppm), there were two amine peaks that had proton chemical shifts located considerably downfield in the proton specrum (16.2 ppm and 15.7 ppm; Figure 7A). Downfield shifts for imidazole protons at the catalytic site in serine proteases have been attributed to the hydrogen bond network of the catalytic triad (Asp81, His57, and Ser139 according to the NS3 protease numbering) [20, 23]. In the presence of boronic acid inhibitors, these protons are shifted even farther downfield, indicating additional stabilization of the Asp-His hydrogen bond [42].

The imidazole resonances were assigned in a ^{1}H-^{15}N long-range HSQC experiment to correlate the $^{15}N\delta1$ and $^{15}N\epsilon2$ chemical shifts with aliphatic $^{1}H\epsilon1$ and $^{1}H\delta2$ protons [43, 44]. This spectrum of ^{15}N NS3/NS4A/InhI in D_2O exhibited sets of peaks for His57 and His149 (Figure 7B). His149 showed nitrogen chemical shifts characteristic of neutral histidine, with a proton residing on the Nϵ2 nitrogen, leaving Nδ1 to complex with the structural zinc [44, 45]. This tautomeric state agrees with previous NMR characterization of His149 in NS3 alone and in NS3 complexed with ketoacid inhibitors [14, 46]. Nitrogen resonances at 181.5 ppm and 181.9 ppm correlated with His57 amine peaks at 16.2/182.6 ppm and 15.7/182.9 ppm in the side chain HSQC (accounting for the deuterium isotope effect). We do not know why there are two sets of peaks for His57, although one explanation is that there are two slightly different conformations at the site of the boronic acid. The backbone amides of residues 137–140, which span the oxyanion hole, also had two sets of peaks with similar chemical shifts. The doubling of peaks is restricted to these immediate neighbors, suggesting that residues with more than one conformation are localized within the region surrounding the oxyanion hole. The $^{15}N\delta1$ and $^{15}N\epsilon2$ chemical shifts for both peaks are characteristic of protonated histidine [20, 45]. Detailed NMR studies on other serine proteases in complex with boronic acid inhibitors have shown that the imidazole chemical shifts clearly distinguish whether the boronic acid forms a histidine or serine adduct, the latter a model of transition state binding [23]. For boronic acid inhibitors in complex with α-lytic protease, the frequency difference between the nitrogens is approximately 30 ppm for histidine adducts and approximately 3 ppm for serine adducts. The 7 ppm frequency difference that is observed for InhI complexed to NS3 is more like a serine adduct.

The pKa of His57 in the NS3/NS4A/InhI complex was determined by acquiring ^{1}H-^{15}N long-range HSQC spectra over a range of pH values (6.5, 7.0, 7.5, 8.1, 9.1, 10.4). At pH $>$ 8, the sample showed significant degradation and peaks were lost in the noise. Throughout the observable pH range, the His57 imidazole chemical shifts were consistent with a protonated histidine, indicating that the pKa of His57 imidazole was greater than 8. In the sidechain HSQC, one amine peak is observed (for each conformation) suggesting that, although the imidazole is protonated, only one amine is in slow enough exchange with water to be observed in the HSQC.

The pKa $>$ 8 for His57 in the NS3/NS4A/InhI complex is consistent with the boronic acid complex acting as a transition-state mimic and with NMR studies of other serine proteases [20]. The pKa of His57 in NS3 alone is close to pH 6.6 [46]. Our results with the boronic acid are in contrast to those reported for ketoacid in complex with NS3 1b where His57 is neutral at physiological pH (pKa $<$ 5.7) [14]. These differences are not surprising since the mechanism of binding of the ketoacid (Figure 1) is considerably different from that expected for the boronic acid inhibitor. Furthermore, the binding of the boronic acid inhibitor is highly dependent on the presence of the NS4A cofactor, as discussed in the following section.

Effect of NS4A on Inhibitor Binding

The relative inhibition constants for InhI in the presence and absence of NS4A ($K_i$app of 13 $\pm$ 2 nM versus 160 $\pm$

35 nM) indicate that the binding of InhI is approximately 10-fold weaker in the absence of cofactor. To identify how the cofactor might influence binding, the ^{1}H-^{15}N HSQC spectrum of NS3/InhI was compared with spectra of NS3 alone and in complex with cofactor, with and without inhibitor (Figure 2). The NS3/InhI spectrum was considerably lower in quality than the other three. Amide peaks for the first 50 residues were substantially shifted, and few could be identified. In contrast, it was possible to assign three-fourths of the backbone amides of the C-terminal domain because in most cases the chemical shifts were similar or identical to those in the ternary complex.

Comparison of the spectra of NS3 and NS3/InhI with and without NS4A gave distinctive insights into the role of this cofactor. First, chemical shifts of many C-terminal domain residues that were sensitive to inhibitor binding (see Figure 5B) showed little or no change in the absence of NS4A. These inhibitor-sensitive, cofactor-insensitive peaks included residues 157–160 in β strand E2, 165–170 in the adjacent strand F2, and residues 132–135 in helix α2. Particularly relevant are the amide peaks for A157 and C159, which in the ternary complex exhibited NOEs to the side chain protons of P_4Val, P_3Val and P_1allyl of the peptide boronic acid inhibitor and showed little change in the absence of cofactor. This suggests that this portion of the inhibitor adopts the same bound conformation as in the ternary complex.

In contrast to the binding of the side chains of the peptide inhibitor, the residues involved in catalysis were very dependent on NS4A binding. A number of peaks at the catalytic site were absent (or extremely weak) in the spectrum of NS3/InhI, including those of residues 56–59 (Figures 2A and 2D) and residues Gly137, Ser138, and Ser139 of the oxyanion hole. Adjacent to this site, resonances of L44, G45, and T46 were not detected in the NS3/InhI complex, even though well-defined peaks were observed in spectra of NS3, NS3/NS4A, and NS3/NS4A/InhI (Figure 8). These resonances, as well as the larger number of other missing peaks in the N-terminal domain, are presumed to be broadened beyond detection. This broadening does not reflect the chemical exchange of inhibitor molecules on and off the protein since the peak intensities and shifts of other inhibitor-sensitive peaks were indicative of complete binding (see G162 in Figure 8). More likely, the loss of peaks adjacent to the catalytic site is indicative of conformational heterogeneity at this site.

In the side chain HSQC of ^{15}N NS3/InhI, the intensity of the catalytic imidazole peaks relative to the backbone amide signals was only one tenth that for the ternary complex. This suggests that although the catalytic site may lack well-defined structure in the absence of cofactor, a fraction of the population may still adopt a transition state binding mode.

The 10-fold loss in binding affinity described above correlates with environmental changes at the catalytic site, whereas the peptide portion of the inhibitor, particularly P_1, P_3, and P_4 sites, is associated with little or no change. Insensitivity to cofactor for the peptide portion of the inhibitor is in agreement with similarities between the solution structure of NS3 1b/ketoacid inhibitor [14] and the crystal structure of NS3 1b/NS4A/ketoacid inhibitor [13] [ketoacid inhibitor is Boc-Glu-Leu-NH-$CH(CH_2CHF_2)C(O)$-COOH]. On the other hand, sensitivity to cofactor at the catalytic site differs from that of the ketoacid binary complex, for which a downfield-shifted His57 Nδ proton indicative of a His57-Asp81 hydrogen bond was observed [14]. It has been pointed out that the cofactor peptide might not have an essential role in the alignment of catalytic residues in the presence of an inhibitor or substrate with a hydrophobic P_2 residue [14]. For the boronic acid inhibitor examined here, with P_2 proline, the NS3 2a catalytic site is indeed sensitive to cofactor. The influence of cofactor on the affinity of protease for inhibitor is consistent with observations made for the NS3 1a single-chain protein, in which the cofactor induced changes at the catalytic site [12]. The cofactor dependence of the boronic acid inhibitor binding parallels changes seen for enzymatic activity, for which the presence of cofactor increases hydrolysis rates ([5, 30, 47, 48] and Figure 4B). Overall, the NMR and enzymatic data are consistent with the boronic acid inhibitor acting as a good mimic for cofactor-dependent substrate hydrolysis.

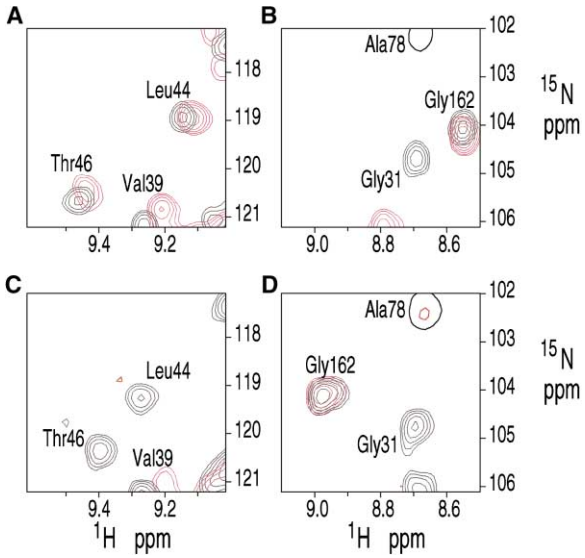

Figure 8. Regions Extracted from ^{1}H-^{15}N HSQC Spectra in Figure 2 Depict How the NS4A Cofactor Influences Inhibitor Binding

(A and B) Spectra of ^{15}N-NS3/NS4A (black) and ^{15}N-NS3 (red) show the effect of cofactor in the absence of inhibitor. (C and D) Spectra of ^{15}N-NS3/NS4A/InhI (black) and ^{15}N-NS3/InhI (red) demonstrate the effect of cofactor with inhibitor bound. (A) Without inhibitor, the amide peaks of Leu44 and Thr46 are largely unaffected by cofactor, (C) whereas with inhibitor bound, they are broadened beyond detection in the absence of cofactor. The amide peak of G162 is unaffected by cofactor and shifts substantially upon inhibitor binding (B and D).

Significance

Careful choice of NS3 and NS4A constructs was critical for obtaining a binary complex in solution under suitable concentrations for NMR and other biophysical studies. NS3 protease from the HCV 2a genotype coupled with a peptide based on NS4A from the HCV 1b

genotype formed stable NS3/NS4A and NS3/NS4A/inhibitor complexes at low glycerol concentrations. NOE and hydrogen exchange data show the essential integration of the cofactor into the N-terminal β sheet of the protease, as has been observed in crystal structures. This solution complex mimics the most active state of the protease and paves the way for high-resolution structure determination of NS3/NS4A complexes in solution.

We examined the binding of a boronic acid inhibitor, Ac-Asp-Glu-Val-Val-Pro-boroAlg-OH (K_i = 13 nM), to NS3 protease with and without bound cofactor. The inhibitor binds in an antiparallel manner to β strand E2 and interacts with the unprimed sites of the substrate binding pocket. Chemical shifts of His57 imidazole nitrogens and pH titration studies demonstrated that, in the NS3/NS4A/inhibitor complex, the inhibitor behaved like a reaction intermediate analog. In the absence of cofactor, inhibitor binding was an order of magnitude weaker. NS3 residues interacting with the peptide portion of the inhibitor showed little change upon binding cofactor, whereas residues adjacent to the catalytic site were highly sensitive to cofactor, suggesting that the lower affinity was due to changes at the catalytic site. The importance of cofactor for transition state-like binding highlights the critical role of cofactor for substrate hydrolysis. Additional structural characterization of NS3/NS4A complexes in solution is needed to understand its role in more detail.

Experimental Procedures

Protein and Peptide Production

RNAzol B (TelTest) was used to extract viral RNA from a sample of HCV 2a-infected human serum. The viral RNA was used as a template for RT/PCR to amplify the NS3 region (amino acids 1027–1218) with the following gene specific primers: CAGCTGCAGCCATGGCC CCCATCACTGCTTAT and CCGAAGCTTTCAAGCAGGTGGTGTGCT GTT. The ends of the amplified fragment were engineered to contain PstI (5′) and HindIII (3′) restriction enzyme sites and a stop codon. After digestion with PstI and HindIII, the DNA fragment was ligated to the PstI and HindIII sites in the vector pTrcHisB (Invitrogen), which provided an amino-terminal histidine tag. Subsequently, the 5′ end was reengineered to contain an NdeI site and amino terminal methionine and subcloned into the NdeI and HindIII sites of the vector pET3AM for expression of the protein without an amino-terminal histidine tag.

An alternative NS3 2a construct [NS3 2a (1–181)Lys_6] was derived by cloning this DNA fragment into the pET24b vector (Novagen) at the NdeI/Hind III site. The NS3 gene was amplified with two PCR primers: a 5′ PCR primer (GGATTCCATATGGCTCCGATCGCTTAC) encoding an NdeI site and amino acids MAPITAY and a 3′ PCR primer (CCCAAGCTTTCACTTTTTCTTTTTCTTTTTCGACCGTGTAG CGATGTCGAGAGA) complementary to amino acid residues 1201–1207. This 3′ primer was followed by a KKKKKK tag, and the stop codon was flanked by a HindIII site. Codons optimized for *E. coli* were used for the first seven N-terminal residues to improve expression levels. Taq DNA polymerase (Life Technology) was used for DNA amplification, and DNA was purified and digested with NdeI and HindIII. The DNA was ligated into the expression vector pET24b with a ligation kit (Pharmacia's Ready-To-Go T4 DNA Ligase) and was sequenced to confirm the construct.

The recombinant vectors were transformed into *E. coli* BL21 (DE3) cells. Cells were grown at 20°C in MOPS minimal media containing $(^{15}NH_4)_2SO_4$, [$^{13}C_6$]glucose or unlabeled glucose, 3.0 g/l labeled Isogro (Isotec), and micronutrients [46]. The protein was purified according to published procedures with minor modifications [46, 49]. In brief, the cells were harvested and resuspended in 1× PBS (pH 7.4), 10% glycerol, 10 mM DTT (dithiothreitol) plus DNase, and 10 mM $MgCl_2$ and were lysed. The supernatant was loaded onto an S-Sepharose FF column (Pharmacia), washed, and eluted at 200 mM NaCl. Fractions containing NS3 were combined, concentrated, and purified by size exclusion chromatography. Pure fractions were combined and dialyzed against NMR buffer and concentrated. The yield of purified protein was 5 mg/l growth.

Isotopically enriched NS4A 1b peptide was expressed in the Novagen's peptide expression system with ketosteroid isomerase (KSI) as a fusion protein tag [50]. Two complementary oligos (with overhangs) were used: AAGAAAGGTTCTGTTGTTATTGTTGGTAGAATT GTTTTATCTGGTAAACCGGCTATCATCCCGAAAAAGATG and CTT TTTCGGGATGATAGCCGGTTTACCAGATAAAACAATTCTACCAAC AATAACAACAGAACCTTTCTTCAT. After phosphorylation with T4 polynucleotide kinase, the two oligos were mixed at a 1:1 ratio and were heated at 99°C for 10 min, 55°C for 3 min, and 30°C for 10 min for complete annealing. The "glassmilk" (Bio101 Mermaid System, Vista, CA) was used for purification of this synthetic mini-gene, which was then ligated into the expression vector pET31b.

KSI-NS4A-His_6 vector was transformed into *E. coli* BL21 (DE3) cells grown at 37°C in MOPS minimal media with $(^{15}NH_4)_2SO_4$ or both $(^{15}NH_4)_2SO_4$ and [$^{13}C_6$]glucose. The peptide was isolated according to published procedures [50]. In brief, the insoluble pellet containing KSI-NS4A-His_6 was suspended in 8M GnHCl, sonicated, and purified on a Ni-NTA column (Qiagen). Fractions containing KSI-NS4A-His_6 were combined and dialyzed against water to precipitate the fusion peptide. The fusion peptide was dissolved in 88% formic acid and cleaved with the addition of cyanogen bromide. The NS4A peptide (KKGSVVIVGRIVLSGKPAIIPKKhS, where "hS" is homoserine) was purified by HPLC.

Mass spectroscopy and N-terminal sequencing were used to confirm all protein and peptide products. ^1H-^{15}N HSQC spectra of the NS3 2a (1–192) and NS3 2a (1–181)Lys_6 were identical (except for the C-terminal residues), indicating that both protein constructs adopted the same structure in solution.

The boronic-acid peptidic inhibitor, Ac-Asp-Glu-Val-Val-Pro-boroAlg-OH, corresponds to the P_6-P_1 cleavage product of the NS5A-NS5B site. The inhibitor was synthesized according to published procedures (C.A.K., S.J., and T.P. Forsyth, peptide boronic acid inhibitors of hepatitis C virus protease, patent WO2001002424, 2001).

NMR Spectroscopy

All NMR experiments were carried out at 25°C on protein [60 μM–1 mM] in sample buffer of 25 mM MES (2-[N-morpholinio]ethanesulfonic acid) buffer (pH 6.5), 100 mM NaCl, 5 mM DTT, and 2% glycerol in 94% H_2O/6% D_2O, unless noted otherwise. Samples were placed in either a 5 mm Shigemi microtube or a 5 mm Wilmad tube. When stored with sodium azide and NS3 inhibitor, samples were stable for months at 4°C.

NMR data were acquired on a four-channel Bruker 600 MHz Avance spectrometer equipped with a Bruker triple resonance, triple axis gradient probe. Chemical shifts were referenced to 10 mM DSS/D_2O at 25°C as described in Wishart et al. [51]. The NMR experimental parameters are listed in Table 2. In all experiments, water magnetization was maintained along the z axis to avoid saturation of protons undergoing exchange [52], and gradients were used to dephase unwanted magnetization [53].

NS3/NS4A/InhI in 94% H_2O/6% D_2O was exchanged into D_2O by diluting the sample 25-fold with D_2O sample buffer, concentrating in a 5K MWCO Biomax (Millipore), then diluting and concentrating again. After the sample was brought to 25°C, a series of ^1H-^{15}N HSQC spectra were acquired to identify protons in slow exchange with water. The D_2O sample was then used for a 2D ^1H-^{15}N long-range HSQC centered at 180 ppm. A 22 ms delay was employed to allow evolution of long-range ^1H_C-^{15}N couplings. A titration of the side chain histidines was obtained by incremental pH adjustments (pH 6.5, 7.0, 7.5, 8.1, 9.1, and 10.4) and 2D ^1H-^{15}N long-range HSQC experiments.

NMR data were processed with nmrPipe [54] processing software and analyzed with nmrWish, PIPP [55] and ANSIG [56, 57] software packages. Peak picking and sorting routines in the PIPP program were used to identify the {H_{Ni}, N_i, $C\alpha_i$, $C\beta_i$} and {H_{Ni}, N_i, $C\alpha_{i-1}$, $C\beta_{i-1}$}

spin systems and to determine the initial sequential backbone assignments. Completion of the backbone assignments and all subsequent data analysis were done with ANSIG and nmrWish.

Enzymology

The peptide substrate, Ac-Asp-Glu-Asp(Edans)-Glu-Glu-AbuΨ[COO]Ala-Ser-Lys(Dabcy)-NH_2, has been described previously for HCV protease [33]. It was prepared by the published procedure. Peptide hydrolysis was measured either by monitoring the appearance of cleavage products by HPLC or by measuring the fluorescence increase that is concurrent with peptide hydrolysis.

For the HPLC assay, NS3 (0.38 nM) was incubated with NS4A (10 μM) for 5 min at 25°C in 50 mM HEPES buffer (pH 7.0) containing 150 mM NaCl, 5 mM DTT, 0.1% maltopyranoside, and 15% glycerol. Substrate was added, and after 10 min, hydrolysis reactions were quenched by the addition of 3.0 μl of 10% TFA to 150 μl reaction solutions. Levels of hydrolysis were determined by HPLC. Aliquots (50 μl) were injected on HPLC, and linear gradients from 90% water, 10% acetonitrile, and 0.1% TFA to 90% acetonitrile were run at a flow rate of 1.0 ml/min over a period of 30 min. HPLCs were run on a HP1090 with a 4.6 $\times$ 250 mm C18 column (Rainin, #83-201-C) equipped with a fluorescent detector with excitation and emission wavelengths set to 350 and 500 nm, respectively. Levels of hydrolysis were determined by measuring the area of the fluorescent peak at 5.3 min. Complete hydrolysis of a 5.0 μM sample gave an area of 3.4 fluorescent units.

Fluorescence assays were conducted under conditions similar to those of the HPLC assays. NS3 was incubated with NS4A for 10 min in 50 mM HEPES buffer (pH 7.0) containing 150 mM NaCl, 5 mM DTT, 0.1% maltopyranoside, and 15% glycerol in a microtiter plate. Reactions were initiated by adding substrate to give a final concentration of 5.0 μM and a total reaction volume of 200 μl. Increases in fluorescence with time were monitored on a SpectraMax Gemini XS spectrofluorometer (Molecular Devices) with excitation and emission wavelengths of 360 and 500 nm, respectively. Rates of hydrolysis in units of fluorescence/s were converted to rates in units of μmol/min/l by measuring the total increase in fluorescence for samples treated with an excess of enzyme. Complete hydrolysis of a 5.0 μM sample gave an increase in fluorescence of 1270 units.

Acknowledgments

We gratefully acknowledge Dale Collins and Nilsa Graciani for peptide synthesis. We thank Haiying Chen and Karl Blom for mass spectrometry analysis, Haiying Chen for assistance with protein purification, and Richard Alexander, Angela Smallwood, Paul Morin, and Carol Budzilowicz for helpful discussions. Thanks are extended to Mark Hixon for early evaluation of NS4A binding and suggestions throughout the project. This paper is DuPont Pharmaceuticals Publication 01P40.

Received: May 31, 2001
Revised: September 21, 2001
Accepted: October 5, 2001

References

1. Tomei, L., Failla, C., Santolini, E., De Francesco, R., and La Monica, N. (1993). NS3 is a serine protease required for processing of hepatitis C virus polyprotein. J. Virol. *67*, 4017–4026.
2. Bartenschlager, R., Ahlborn-Laake, L., Mous, J., and Jacobsen, H. (1993). Nonstructural protein 3 of the hepatitis C virus encodes a serine-type proteinase required for cleavage at the NS3/4 and NS4/5 junctions. J. Virol. *67*, 3835–3844.
3. Grakoui, A., McCourt, D.W., Wychowski, C., Feinstone, S.M., and Rice, C.M. (1993). Characterization of the hepatitis C virus-encoded serine proteinase: determination of proteinase-dependent polyprotein cleavage sites. J. Virol. *67*, 2832–2843.
4. Failla, C., Tomei, L., and De Francesco, R. (1994). Both NS3 and NS4A are required for proteolytic processing of hepatitis C virus nonstructural proteins. J. Virol. *68*, 3753–3760.
5. Butkiewicz, N.J., Wendel, M., Zhang, R., Jubin, R., Pichardo, J., Smith, E.B., Hart, A.M., Ingram, R., Durkin, J., Mui, P.W., et al. (1996). Enhancement of hepatitis C virus NS3 proteinase activity by association with NS4A-specific synthetic peptides: identification of sequence and critical residues of NS4A for the cofactor activity. Virology *225*, 328–338.
6. Kim, J.L., Morgenstern, K.A., Lin, C., Fox, T., Dwyer, M.D., Landro, J.A., Chambers, S.P., Markland, W., Lepre, C.A., et al. (1996). Crystal structure of the hepatitis C virus NS3 protease domain complexed with a synthetic NS4A cofactor peptide. Cell *87*, 343–355.
7. Yan, Y., Li, Y., Munshi, S., Sardana, V., Cole, J.L., Sardana, M., Steinkuehler, C., Tomei, L., De Francesco, R., Kuo, L.C., et al. (1998). Complex of NS3 protease and NS4A peptide of BK strain hepatitis C virus: a 2.2 Å resolution structure in a hexagonal crystal form. Protein Sci. *7*, 837–847.
8. Love, R.A., Parge, H.E., Wickersham, J.A., Hostomsky, Z., Habuka, N., Moomaw, E.W., Adachi, T., Margosiak, S., Dagostino, E., and Hostomska, Z. (1998). The conformation of hepatitis C virus NS3 proteinase with and without NS4A: a structural basis for the activation of the enzyme by its cofactor. Clin. Diagn. Virol. *10*, 151–156.
9. Yao, N., Reichert, P., Taremi, S.S., Prosise, W.W., and Weber, P.C. (1999). Molecular views of viral polyprotein processing revealed by the crystal structure of the hepatitis C virus bifunctional protease-helicase. Struct. Fold. Des. *7*, 1353–1363.
10. Love, R.A., Parge, H.E., Wickersham, J.A., Hostomsky, Z., Habuka, N., Moomaw, E.W., Adachi, T., and Hostomska, Z. (1996). The crystal structure of hepatitis C virus NS3 proteinase reveals a trypsin-like fold and a structural zinc binding site. Cell *87*, 331–342.
11. Barbato, G., Cicero, D.O., Nardi, M.C., Steinkuhler, C., Cortese, R., De Francesco, R., and Bazzo, R. (1999). The solution structure of the N-terminal proteinase domain of the hepatitis C virus (HCV) NS3 protein provides new insights into its activation and catalytic mechanism. J. Mol. Biol. *289*, 371–384.
12. McCoy, M.A., Senior, M.M., Gesell, J.J., Ramanathan, L., and Wyss, D.F. (2001). Solution structure and dynamics of the single-chain hepatitis C virus NS3 protease NS4A cofactor complex. J. Mol. Biol. *305*, 1099–1110.
13. Di Marco, S., Rizzi, M., Volpari, C., Walsh, M.A., Narjes, F., Colarusso, S., De Francesco, R., Matassa, V.G., and Sollazzo, M. (2000). Inhibition of the hepatitis C virus NS3/4A protease. The crystal structures of two protease-inhibitor complexes. J. Biol. Chem. *275*, 7152–7157.
14. Barbato, G., Cicero, D.O., Cordier, F., Narjes, F., Gerlach, B., Sambucini, S., Grzesiek, S., Matassa, V.G., De Francesco, R., and Bazzo, R. (2000). Inhibitor binding induces active site stabilization of the HCV NS3 protein serine protease domain. EMBO J. *19*, 1195–1206.
15. Schecter, I., and Berger, A. (1967). On the size of the active site in proteases. I. Pain. Biochem. Biophys. Res. Commun. *27*, 157–162.
16. Håkansson, K., Tulinsky, A., Abelman, M.M., Miller, T.A., Vlasuk, G.P., Bergum, P.W., Lim-Wilby, M.S.L., and Brunck, T.K. (1995). Crystallographic structure of a peptidyl keto acid inhibitor and human alpha-thrombin. Bioorg. Med. Chem. *3*, 1009–1017.
17. Schloss, J.V., and Cleland, W.W. (1982). Inhibition of isocitrate lyase by 3-nitropropionate, a reaction-intermediate analog. Biochemistry *21*, 4420–4427.
18. Walter, J., and Bode, W. (1983). The X-ray crystal structure analysis of the refined complex formed by bovine trypsin and *p*-amidinopenylpyruvate at 1.4 Å resolution. Hoppe Seylers Z. Physiol. Chem. *364*, 949–959.
19. Bone, R., Shenvi, A.B., Kettner, C.A., and Agard, D.A. (1987). Serine protease mechanism: structure of an inhibitory complex of a lytic protease and a tightly bound peptide boronic acid. Biochemistry *26*, 7609–7614.
20. Bachovchin, W.W., Wong, W.Y., Farr-Jones, S., Shenvi, A.B., and Kettner, C.A. (1988). Nitrogen-15 NMR spectroscopy of the catalytic-triad histidine of a serine protease in peptide boronic acid inhibitor complexes. Biochemistry *27*, 7689–7697.
21. Zhong, S., Jordan, F., Kettner, C., and Polgar, L. (1991). Observation of tightly bound 11B nuclear magnetic resonance signal on serine proteases: direct solution evidence for tetrahedral

geometry around the boron in the putative transition state analogues. J. Am. Chem. Soc. *113*, 9429–9435.
22. Tsilikounas, E., Kettner, C.A., and Bachovchin, W.W. (1993). 11B NMR spectroscopy of peptide boronic acid inhibitor complexes of alpha-lytic protease. Direct evidence for tetrahedral boron in both boron-histidine and boron-serine adduct complexes. Biochemistry *32*, 12651–12655.
23. Tsilikounas, E., Kettner, C.A., and Bachovchin, W.W. (1992). Identification of serine and histidine adducts in complexes of trypsin and trypsinogen with peptide and nonpeptide boronic acid inhibitors by 1H NMR spectroscopy. Biochemistry *31*, 12839–12846.
24. Urbani, A., Bianchi, E., Narjes, F., Tramontano, A., De Francesco, R., Steinkuhler, C., and Pessi, A. (1997). Substrate specificity of the hepatitis C virus serine protease NS3. J. Biol. Chem. *272*, 9204–9209.
25. Lee, J.-H., Bang, K., Jung, J.-W., Ahn, I.-A., Ro, S., and Lee, W. (1999). Solution conformation of the substrates and inhibitor of hepatitis C virus NS3 protease. Bull. Korean Chem. Soc. *20*, 301–306.
26. LaPlante, S.R., Cameron, D.R., Aubry, N., Lefebvre, S., Kukolj, G., Maurice, R., Thibeault, D., Lamarre, D., and Llinas-Brunet, M. (1999). Solution structure of substrate-based ligands when bound to hepatitis C virus NS3 protease domain. J. Biol. Chem. *274*, 18618–18624.
27. Cicero, D.O., Barbato, G., Koch, U., Ingallinella, P., Bianchi, E., Nardi, M.C., Steinkuhler, C., Cortese, R., Matassa, V., De Francesco, R., et al. (1999). Structural characterization of the interactions of optimized product inhibitors with the N-terminal proteinase domain of the hepatitis C virus (HCV) NS3 protein by NMR and modelling studies. J. Mol. Biol. *289*, 385–396.
28. LaPlante, S.R., Aubry, N., Bonneau, P.R., Kukolj, G., Lamarre, D., Lefebvre, S., Li, H., Llinas-Brunet, M., Plouffe, C., and Cameron, D.R. (2000). NMR line-broadening and transferred NOESY as a medicinal chemistry tool for studying inhibitors of the hepatitis C virus NS3 protease domain. Bioorg. Med. Chem. Lett. *10*, 2271–2274.
29. Bodenhausen, G., and Ruben, D.J. (1980). Natural abundance nitrogen-15 NMR by enhanced heteronuclear spectroscopy. Chem. Phys. Lett. *69*, 185–189.
30. Bianchi, E., Urbani, A., Biasiol, G., Brunetti, M., Pessi, A., De Francesco, R., and Steinkuhler, C. (1997). Complex formation between the hepatitis C virus serine protease and a synthetic NS4A cofactor peptide. Biochemistry *36*, 7890–7897.
31. Urbani, A., Biasiol, G., Brunetti, M., Volpari, C., Di Marco, S., Sollazzo, M., Orru, S., Piaz, F.D., Casbarra, A., Pucci, P., et al. (1999). Multiple determinants influence complex formation of the hepatitis C virus NS3 protease domain with its NS4A cofactor peptide. Biochemistry *38*, 5206–5215.
32. Wright-Minogue, J., Yao, N., Zhang, R., Butkiewicz, N.J., Baroudy, B.M., Lau, J.Y., and Hong, Z. (2000). Cross-genotypic interaction between hepatitis C virus NS3 protease domains and NS4A cofactors. J. Hepatol. *32*, 497–504.
33. Taliani, M., Bianchi, E., Narjes, F., Fossatelli, M., Urbani, A., Steinkuhler, C., Defrancesco, R., and Pessi, A. (1996). A continuous assay of hepatitis C virus protease based on resonance energy transfer depsipeptide substrates. Anal. Biochem. *240*, 60–67.
34. Clore, G.M., and Gronenborn, A.M. (1991). Structures of larger proteins in solution: three- and four-dimensional heteronuclear NMR spectroscopy. Science *252*, 1390–1399.
35. Bax, A., and Grzesiek, S. (1993). Methodological advances in protein NMR. Acc. Chem. Res. *26*, 131–138.
36. Wishart, D.S., and Sykes, B.D. (1994). The 13C chemical shift index: a simple method for the identification of protein secondary structure using 13C chemical shift data. J. Biomol. NMR *4*, 171–180.
37. Taremi, S.S., Beyer, B., Maher, M., Yao, N., Prosise, W., Weber, P.C., and Malcolm, B.A. (1998). Construction, expression, and characterization of a novel fully activated recombinant single-chain hepatitis C virus protease. Protein Sci. *7*, 2143–2149.
38. Bianchi, E., Orru, S., Dal Piaz, F., Ingenito, R., Casbarra, A., Biasiol, G., Koch, U., Pucci, P., and Pessi, A. (1999). Conformational changes in human hepatitis C virus NS3 protease upon binding of product-based inhibitors. Biochemistry *38*, 13844–13852.
39. Davis, J.H., Agard, D.A., Handel, T.M., and Basus, V.J. (1997). Alterations in chemical shifts and exchange broadening upon peptide boronic acid inhibitor binding to alpha-lytic protease. J. Biomol. NMR *10*, 21–27.
40. Weiner, P.K., and Kollman, P.A. (1981). AMBER: assisted model building with energy refinement. J. Comput. Chem. *2*, 287–303.
41. Weiner, S.J., Kollman, P.A., Case, D.A., Singh, U.C., Ghio, C., Algona, G., Profeta, S.J., and Weiner, P.A. (1984). A new force field for molecular mechanical simulation of nucleic acids and proteins. J. Am. Chem. Soc. *106*, 765–784.
42. Bao, D., Huskey, P., Kettner, C.A., and Jordan, F. (1999). Hydrogen bonding to active-site histidine in peptidyl boronic acid inhibitor complexes of chymotrypsin and subtilisin: proton magnetic resonance assignments and H/D fractionation. J. Am. Chem. Soc. *121*, 4684–4689.
43. Bax, A., and Summers, M.F. (1986). 1H and 13C assignments from sensitivity enhanced detection of multiple bond CH connectivity by two-dimensional multiple quantum NMR. J. Am. Chem. Soc. *108*, 2093–2094.
44. Pelton, J.G., Torchia, D.A., Meadow, N.D., and Roseman, S. (1993). Tautomeric states of the active-site histidines of phosphorylated and unphosphorylated IIIGlc, a signal-transducing protein from E. coli, using two-dimensional heteronuclear NMR techniques. Protein Sci. *2*, 543–558.
45. Bachovchin, W.W. (1986). 15N NMR spectroscopy of hydrogen-bonding interactions in the active site of serine proteases: evidence for a moving histidine mechanism. Biochemistry *25*, 7751–7759.
46. Urbani, A., Bazzo, R., Nardi, M.C., Cicero, D.O., De Francesco, R., Steinkuhler, C., and Barbato, G. (1998). The metal binding site of the hepatitis C virus NS3 protease. A spectroscopic investigation. J. Biol. Chem. *273*, 18760–18769.
47. Landro, J.A., Raybuck, S.A., Luong, Y.P.C., O'Malley, ET, Harbeson, S.L., Morgenstern, K.A., Rao, G., and Livingston, D.J. (1997). Mechanistic role of an NS4A peptide cofactor with the truncated NS3 protease of hepatitis C virus: elucidation of the NS4A stimulatory effect via kinetic analysis and inhibitor mapping. Biochemistry *36*, 9340–9348.
48. Gallinari, P., Paolini, C., Brennan, D., Nardi, C., Steinkuhler, C., and De Francesco, R. (1999). Modulation of hepatitis C virus NS3 protease and helicase activities through the interaction with NS4A. Biochemistry *38*, 5620–5632.
49. De Francesco, R., Urbani, A., Nardi, M.C., Tomei, L., Steinkuhler, C., and Tramontano, A. (1996). A zinc binding site in viral serine proteinases. Biochemistry *35*, 13282–13287.
50. Kuliopulos, A., and Walsh, C. (1994). Production, purification, and cleavage of tandem repeats of recombinant peptides. J. Am. Chem. Soc. *116*, 4599–4607.
51. Wishart, D.S., Bigam, C.G., Yao, J., Abildgaard, F., Dyson, H.J., Oldfield, E., Markley, J.L., and Sykes, B.D. (1995). 1H, 13C and 15N chemical shift referencing in biomolecular NMR. J. Biomol. NMR *6*, 135–140.
52. Stonehouse, J., Clowes, R.T., Shaw, G.L., Keeler, J., and Laue, E.D. (1995). Minimisation of sensitivity losses due to the use of gradient pulses in triple-resonance NMR of proteins. J. Biomol. NMR *5*, 226–232.
53. Bax, A., and Pochapsky, S.S. (1992). Optimized recording of heteronuclear multidimensional NMR spectra using pulsed field gradients. J. Magn. Reson. *99*, 638–643.
54. Delaglio, F., Grzesiek, S., Vuister, G.W., Zhu, G., Pfeifer, J., and Bax, A. (1995). NMRPipe: a multidimensional spectral processing system based on UNIX pipes. J. Biomol. NMR *6*, 277–293.
55. Garrett, D.S., Powers, R., Gronenborn, A.M., and Clore, G.M. (1991). A common sense approach to peak picking in two-, three-, and four-dimensional spectra using automatic computer analysis of contour diagrams. J. Magn. Reson. *95*, 214–220.
56. Kraulis, P.J. (1989). ANSIG: a program for the assignment of protein 1H 2D NMR spectra by interactive graphics. J. Magn. Reson. *84*, 627–633.
57. Kraulis, P.J., Domaille, P.J., Campbell-Burk, S.L., Aken, T.V., and Laue, E.D. (1994). Solution structure and dynamics of ras

p21-GDP determined by heteronuclear three- and four-dimensional NMR spectroscopy. Biochemistry *33*, 3515–3531.

58. Kraulis, P. (1991). MOLSCRIPT, a program to produce both detailed and schematic plots of protein structures. J. Appl. Crystallogr. *24*, 946–950.
59. Merritt, E.A., and Bacon, D.J. (1997). Raster3D: photorealistic molecular graphics. Methods Enzymol. *277*, 505–524.
60. Bax, A., Ikura, M., Kay, L.E., Torchia, D.A., and Tschudin, R. (1990). Comparison of different modes of two-dimensional reverse-correlation NMR for the study of proteins. J. Magn. Reson. *86*, 304–318.
61. Grzesiek, S., and Bax, A. (1992). Correlating backbone amide and side chain resonances in larger proteins by multiple relayed triple resonance NMR. J. Am. Chem. Soc. *114*, 6291–6293.
62. Muhandiram, D.R., and Kay, L.E. (1994). Gradient-enhanced triple-resonance three-dimensional NMR experiments with improved sensitivity. J. Magn. Reson. B. *103*, 203–216.
63. Grzesiek, S., and Bax, A. (1992). An efficient experiment for sequential backbone assignment of medium-sized isotopically enriched proteins. J. Magn. Reson. *99*, 201–207.
64. Wittekind, M., and Mueller, L. (1993). HNCACB, a high-sensitivity 3D NMR experiment to correlate amide-proton and nitrogen resonances with the alpha- and beta-carbon resonances in proteins. J. Magn. Reson. B *101*, 201–205.
65. Yamazaki, T., Lee, W., Arrowsmith, C.H., Muhandiram, D.R., and Kay, L.E. (1994). A suite of triple resonance NMR experiments for the backbone assignment of ^{15}N,^{13}C,^{2}H-labeled proteins with high sensitivity. J. Am. Chem. Soc. *116*, 11655–11666.
66. Kay, L.E., Ikura, M., Tschudin, R., and Bax, A. (1990). Three-dimensional triple-resonance NMR spectroscopy of isotopically enriched proteins. J. Magn. Reson. *89*, 496–514.
67. Yamazaki, T., Lee, W., Revington, M., Mattiello, D.L., Dahlquist, F.W., Arrowsmith, C.H., and Kay, L.E. (1994). An HNCA pulse scheme for the backbone assignment of ^{15}N,^{13}C,^{2}H-labeled proteins: application to a 37-kDa Trp repressor-DNA complex. J. Am. Chem. Soc. *116*, 6464–6465.
68. Ikura, M., and Bax, A. (1992). Isotope-filtered 2D NMR of a protein-protein complex: study of a skeletal muscle myosin light chain kinase fragment bound to calmodulin. J. Am. Chem. Soc. *114*, 2433–2440.